Revisiting the Fluorescence of Benzothiadiazole Derivatives: Anti-Kasha Emission or Not?

*Koen Veys [a], Flip de Jong [a], Annelies Adriaens [a], Gitte Coenen [a], Kylie Coenen [a], Yvonne De Ligt [a], Quinten Meysman [a], Trijntje Paredis [a], Jesse Stalmans [a], Prof. Dr. Wim Dehaen [a], Prof. Dr. Mark Van der Auweraer [a], Prof. Dr. Daniel Escudero [a]**

[a]Department of Chemistry, KU Leuven, Celestijnenlaan 200F, B-3001 Leuven, Belgium

*Corresponding author

Email address: daniel.escudero@kuleuven.be **– Tel. +32 16 19 33 53 –**

https://danielescuderomasa.wixsite.com/website

ABSTRACT

In this paper we revisit the fluorescent properties of two fluorophores, namely N-butyl-7-(4-methoxyphenyl)-2,1,3-benzothiadiazole-4-amine (**1**) and 4-[[7-(4-methoxyphenyl)-2,1,3-benzothiadiazole-4-yl]amino]-benzonitrile (**2**), whose emissive and fluorescent sensing properties were recently investigated by Peng *et al.* in [1]. Experimentally, these two fluorophores were reported to show excitation wavelength-dependent emission properties, especially **1**, which is a dual emitter. The authors of the original manuscript ascribed the excitation-wavelength dependent emission properties to an emission from a higher-lying excited state (i.e. anti-Kasha emission). Our investigations, including steady-state spectroscopy, lifetime measurements and time-dependent density functional theory and second-order algebraic diagrammatic construction [ADC(2)] calculations, unambiguously highlight that the fluorophores do not violate Kasha's rule but reveal instead that a protonated species is responsible for the higher-lying emissive band. In addition, we have elucidated the actual fluorescent pH sensing mechanisms. More and more molecular systems are reported to violate Kasha's rule; sometimes without compelling proof. This study highlights the need to i) exhaustively investigate apparent anomalous cases reported in the literature that seemingly violate Kasha's rule and ii) propose good scientific practices to correctly assign anomalous photochemical events.

INTRODUCTION

The lowest excited states of molecular systems (S_1 and/or T_1) are very often responsible for their photochemical reactivity as well as for their emissive properties; that is these molecular systems

behave in a Kasha-like manner. In this regard, in 1950, Michael Kasha formulated the so-called Kasha's rule, i.e., "the emitting electronic level of a given multiplicity is the lowest excited level of that multiplicity".[2] Later, Kasha's rule was reformulated as "polyatomic molecular entities react with appreciable yield only from the lowest excited state of a given multiplicity".[3,4] Already in the 1950's, the first violations of Kasha's rule were reported. Specifically, for azulene, anti-Kasha emission from its second excited state (S_2) was demonstrated.[5] During the 1970's many other molecular systems were reported to behave in an anti-Kasha manner.[6] Among the reported cases, other types of anomalous emissions, such as e.g., those arising from hot vibronic states and/or from close-lying thermally-equilibrated excited states, were reported.[7] Although some of these cases do not strictly represent Kasha's rule violations, they showcase the often complex excited-state dynamics of molecular systems at different timescales. In this regard, excited state processes are kinetically-controlled and thus, the outcomes of photochemical reactions are controlled by a subtle interplay of photodeactivation processes, among which the most predominant are vibrational relaxation, internal conversion, intersystem crossing processes and radiative deactivation. Besides their fundamental interest, anti-Kasha photochemical events have also great prospects to be used for technological applications because of their more efficient energy conversions as compared with Kasha-like photoprocesses.[8]

Since the work of Kasha, Turro and others; many experimental[7] and theoretical/computational[9,10] efforts have been devoted to put on firmer grounds truly anti-Kasha events, but also to disclose other types of anomalous emissive scenarios strictly not violating Kasha's rule according to its IUPAC's formulation.[4] Despite the strong pieces of evidence for Kasha's rule violations in a wide

variety of molecular systems, some of them still raise some controversy among the community.[11] In this regard, a putative anti-Kasha photochemical process might erroneously be assigned if other sources of typical footprints for anti-Kasha photochemistry are not strictly ruled out. Among these other possible sources of Kasha-like footprints we hereby highlight the following: impurities and subproducts, reactions/photoreactions (for instance tautomerism reactions), different excited conformers on the S_1 potential energy surface, but also condensed-phase events such as e.g., up-conversion emission. The above processes may lead to the wrong assignment of anti-Kasha events and thus, any putative anti-Kasha scenario requires exhaustive steady-state and time-resolved spectroscopic investigations, ideally accompanied by theoretical/computational investigations.

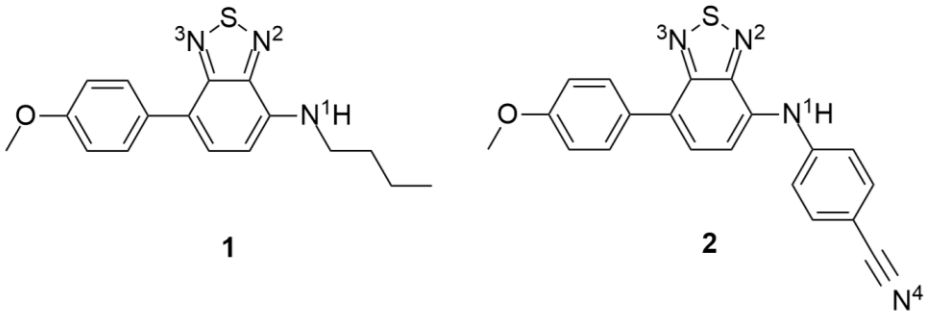

*Scheme 1. Molecular structures of **1** and **2** with possible protonation sites.*

The benzothiadiazole (BTD) derivatives shown in Scheme 1, namely N-butyl-7-(4-methoxyphenyl)-2,1,3-benzothiadiazole-4-amine (**1**) and 4-[[7-(4-methoxyphenyl)-2,1,3-benzothiadiazole-4-yl]amino]-benzonitrile (**2**), were recently investigated by Peng *et al.*[1] Experimentally, **1**-**2** were reported to show excitation wavelength-dependent emission properties in toluene and acetonitrile, which is a typical footprint for anti-Kasha behavior, but also dual fluorescence.[12] As far as we know, even though BTD derivatives are investigated as OLED

candidates, this is the first report of anti-Kasha fluorescence for these compounds.[13,14] Especially in the case of **1** this was pronounced: when exciting the samples with an excitation wavelength of 500 nm they recorded emission at 623 nm while when exciting with 360 nm an anomalous emission at 547 nm was recorded. The authors of the original manuscript ascribed the anomalous emission to an emission from a higher-lying excited state (i.e., anti-Kasha emission) but no compelling experimental and/or computational proof was provided. In this manuscript we revisit the photophysical properties of **1**-**2** with an exhaustive combination of experimental and computational investigations. The presence/absence of impurities of subproducts is ruled out through purification of the synthesized samples. Analogously, the condensed-phase events were experimentally ruled out by working at different conditions and especially at very diluted concentrations (~10^{-5} M). The benzothiadiazole derivatives possess nitrogens in several positions, susceptible to protonation in their ground or excited states. Herein, we investigate all possible tautomeric species of **1**-**2** (see Scheme S1 in the supporting information**)**, as well as other photoreactions, such as e.g., the excited-state intramolecular proton transfer (ESIPT) reaction or proton transfer with a solvent molecule; depicted in Scheme S1. In addition, a putative emission from a higher-lying singlet excited state (S_2) has been theoretically investigated with the help of time-dependent density functional theory (TDDFT) and second-order algebraic diagrammatic construction [ADC(2)] calculations. These calculations were augmented with excitation-emission maps and fluorescence decay traces of **1** in toluene and acetonitrile with and without the addition of an acid. Together, these investigations unambiguously assign the origin of the anomalous emission to a protonated form of **1**. Once the photophysical properties of **1**-**2** were put on firmer grounds this has permitted to revisit the fluorescent sensing properties of the fluorophores.

Accordingly, **1** can be used as a pH sensing fluorescent probe, even though it does not show anti-Kasha fluorescence.

EXPERIMENTAL SECTION

Synthesis

Both products were synthesized according to ref [1], starting with the synthesis of the intermediate product 4-bromo-7-(4-methoxyphenyl)benzo[c][1,2,5]thiadiazole by using 0.87 g of 4,7-dibromobenzo[c][1,2,5]thiadiazole. The Suzuki reaction with 4-methoxyphenylboronic acid was followed by thin layer chromatography (TLC) and was quenched after 225 minutes, when no starting product was visible anymore. The intermediate product was purified by column chromatography on silica gel using dichloromethane/heptane (1:2) as eluent, obtaining a yield of 48%. The syntheses of **1** and **2** were performed by Buchwald-Hartwig substitution reaction of the intermediate with the appropriate amine without any modifications to the original procedure. Characterization of all substances was performed with ^{1}H-NMR. (See Figure S1 and S2 in the supporting information.)

Spectroscopy

Absorbance spectra were measured with a Perkin Elmer Lambda 950 UV-VIS spectrometer, while excitation/emission spectra were measured with a Horiba Jobin fluorimeter Fluorolog FL3-22. The emission spectra were corrected for the wavelength dependence of the sensitivity of the detection channel. Quartz cuvettes with a path length of 1 cm were used for these measurements. To obtain

the absolute quantum yield (QY), an integrating sphere accessory was used in the same fluorimeter and the solutions were measured in cylindrical quartz cuvettes. For recording the Rayleigh scatter a neutral density filter of 0.3% was used. The details of the time-correlated single-photon counting (TC-SPC) setup were recently published by our group.[15]

Computational

All ground and excited states were optimized with respectively density functional theory[16–18] (DFT) and TDDFT[19,20], using 6-31+G(d)[21] and CAM-B3LYP[22] as basis set and functional. For each optimized structure, a frequency calculation was performed to check for the absence of imaginary frequencies. The transition state between **1**P^+(N^1) and **1**P^+(N^2) (optimized using the Berny algorithm[23]) was confirmed by having one imaginary frequency. The integral equation formalism variant of the Polarizable Continuum Model (IEFPCM) was used to account for solvent effects (toluene and acetonitrile).[24] The quality of the computed TDDFT energies was assessed with ADC(2)[25] calculations, using the def2-TZVP basis set[26]. The latter calculations were performed with Turbomole v7.1[27], while Gaussian rev.16A03[28] was used for all other calculations.

RESULTS AND DISCUSSION

The steady-state spectroscopy results are summarized in Table 1. While the absorption data largely corresponded to the results of Peng *et al.*[1] (within ~1 nm), the emission maxima showed deviations up to ~60 nm (0.2 eV). For **1**, the absorption maximum shows no significant change when going from toluene to acetonitrile, although the emission maximum shows a red shift of 35 nm (0.1 eV). For **2**, the emission shows a similar red shift (0.08 eV), but the absorption shows a blue shift (0.08

eV), probably caused by a better MeCN-solvation of **2** compared to **1** in the ground state. The red shift of the emission in MeCN observed for both **1** and **2** suggests the presence of an excited state dipole moment. This is confirmed by the increase of the Stokes shift in MeCN observed for both **1** and **2**. The blue shift of the absorption spectrum of **2** in MeCN is due to the smaller polarizability of MeCN compared to toluene. Such shifts of about 10 nm between on the one hand non polarizable solvents (ethanol, MeCN) and on the other hand polarizable solvents such as toluene or $CHCl_3$ have been observed for several molecules with no ground state dipole moment.[29–31] For the absorption spectrum of **1** in MeCN the red shift related to the presence of the small dipole moment in the ground state is cancelled by the effect of the smaller solvent polarizability.

*Table 1. Experimental absorption (abs) and emission (emi) maxima; Stokes' shift ($\bar{\nu}_{abs} - \bar{\nu}_{emi}$); full width at half maximum of emission band ($FWHM_{emi}$); fluorescence quantum yield (ϕ) and extinction coefficient (ε) for **1**; protonated **1** and **2** in Toluene (Tol) and acetonitrile (MeCN).*

	Solvent	$\lambda_{abs,exp}$ (nm)	$\lambda_{emi,exp}$ (nm)	$\bar{\nu}_{abs} - \bar{\nu}_{emi}$ **(10^3 cm^{-1})**	**FWHM**$_{emi}$ (10^3 cm^{-1})	**φ**	**ε** (10^4 M^{-1}cm^{-1})
1	Tol	470	653	6.0	3.1	0.04	3.7
	MeCN	469	688	6.8	3.0	<0.005	8.6
1P$^+$	MeCN	379	579	9.1	6.4	0.11	8.2
2	Tol	460	584	4.6	2.5	0.35	1.6
	MeCN	447	607	5.9	3.7	0.06	1.7

To investigate the double emission in more detail, 2D excitation-emission plots were recorded for **1** and **2** (Figure 1). For **1** in toluene, there are clearly two distinct emission bands with different excitation spectra, already indicating the presence of two different species. A first species is responsible for the long wavelength absorption band with maximum at 470 nm and emitting at 653 nm, while there is a second species with absorption around 375 nm and an emission maximum around 500 nm. In MeCN the band at longer wavelength is much less pronounced in the emission

map but it is still present (see also the excitation spectra in panel D) while the emission of the short wavelength band shifted to 550 nm. After addition of trifluoroacetic acid (TFA), only the two short wavelength peaks remain. In MeCN the emission maximum shifted about 20 nm to longer wavelengths while the excitation maximum shifted about 10 nm to longer wavelength. This is a first indication that the origin of this extra peak is probably a protonated form of **1**. Comparing the absorption and excitation spectra of **1** in both MeCN and toluene in Figure 1D, it is clear that the emission at longer wavelengths must be attributed to the species yielding the major absorption band around 470 nm. The emission band at shorter wavelengths on the other hand has to be attributed to a minor species not visible in the absorption spectrum. This discrepancy between the contribution of this short wavelength species to the absorption and emission spectra suggests that it has a significantly higher fluorescent quantum yield. The similarity between the absorption spectrum of **1**P^+ in MeCN and the excitation spectra of this short-wavelength band in toluene and MeCN further supports our hypothesis that a protonated species is responsible for the presumed anti-Kasha emission. Furthermore, a control experiment with the subsequent addition of the base triethylamine to toluene resulted in a reduced emission of the protonated species (Figure S3) while the intensity of the long wavelength emission did not change significantly. This indicated that the protonation was reversible and could make **1** suitable as a pH sensor. A spectrophotometric titration of **1** in MeCN with TFA was carried out (Figure S4) and is shown to be consistent with a single protonation step. In a next step we recorded the fluorescence decays of the different observed bands in toluene and MeCN. Peng *et al.* reported bi-exponential decays in toluene for both bands, we however obtained mono-exponential decays (Table 2, fits are given in Figure S5) except for the long wavelength band in MeCN, where there is still a very small contribution of the

short wavelength species. For **1** in toluene, we recovered a lifetime of 11.1 ns at 500 nm and a lifetime of 1.9 ns at 650 nm, which is close to the 1.32 and 10.96 ns lifetimes reported by Peng et al. at 483 nm. At 595 nm they report a component of 1.65 ns and a component of 4.85 ns, the deviating value of the latter is probably due to the low signal to noise ratio in the tail of the fluorescence decay they observed. From the fluorescence quantum yield of the long wavelength emission of **1** (0.04) and its fluorescent decay time (1.9 ns) a fluorescent rate constant of 2.1×10^7 s^{-1} can be calculated. The latter corresponds to an oscillator strength of 0.03. When the emission was observed at 550 nm the fluorescence decay of **1** in MeCN could be analyzed as single exponential decay and a decay time of 16 ns was recovered, which is slightly longer than the 11.1 ns recovered for the fluorescence decay of the short wavelength species in toluene. At 700 nm the fluorescence decay of **1** in MeCN has to be analyzed as a bi-exponential decay with a major component with decay time of 0.29 ns, attributed to the long wavelength species and minor component with a decay time of 16.0 ns attributed to the tail of the emission spectrum of the short wavelength species. The decay time of the long wavelength species is more than six times smaller than in toluene. Assuming the same fluorescent rate constant this would correspond to a fluorescent quantum yield of less than 1 % which is 10 times smaller than that of **1** in MeCN in the presence of TFA, consistent with what is observed. After addition of TFA only one decay time of 4.76 ns can be observed both at 550 and 700 nm.

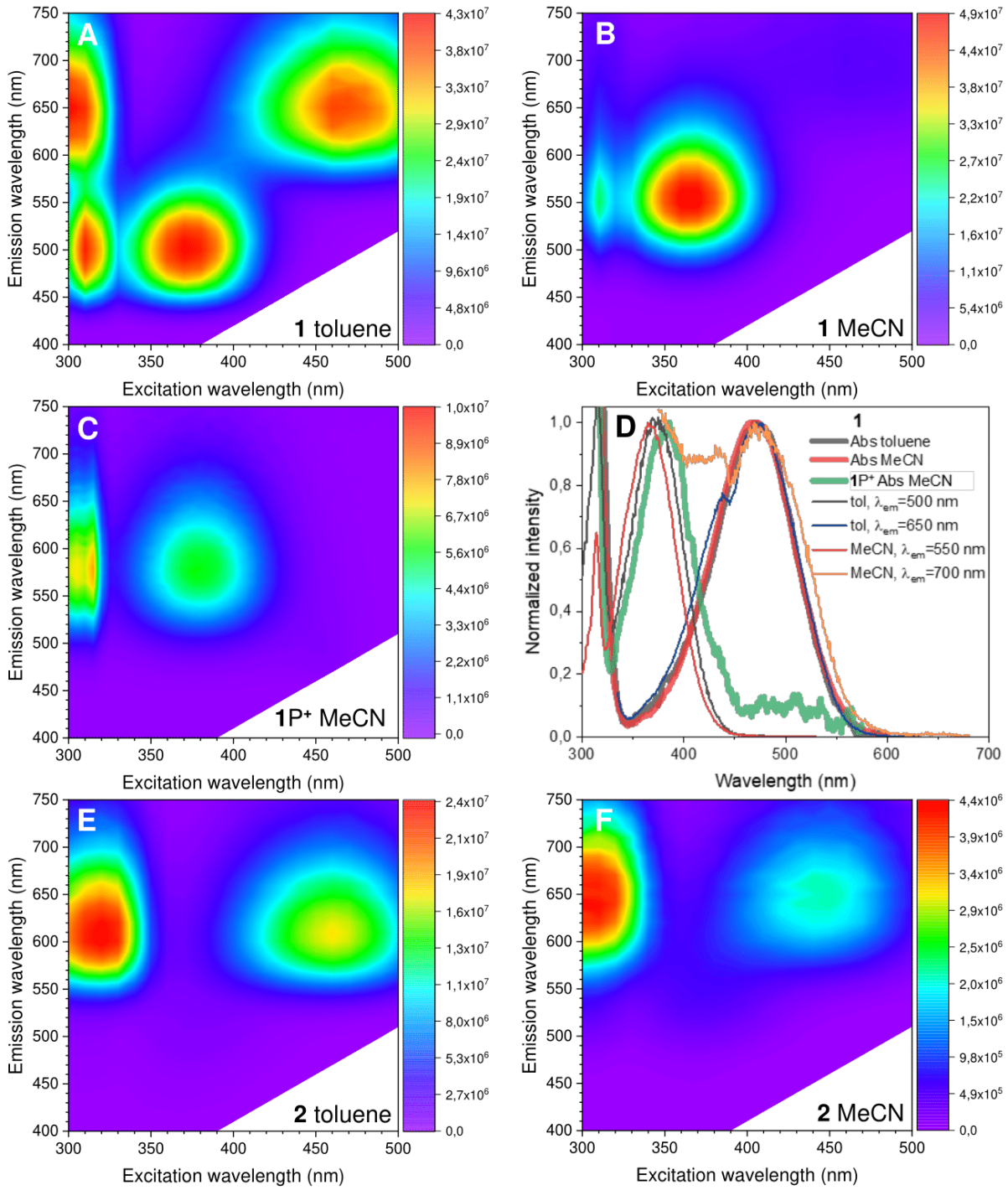

*Figure 1. Excitation-emission maps of **1** in toluene (A), MeCN (B) and MeCN acidified with TFA (C). (D) Comparison of the absorption spectra of **1** and **1P**⁺ with excitation spectra of the different bands of **1** in toluene and MeCN. Excitation-emission maps of **2** in toluene (E) and MeCN (F).*

Table 2. Decay times (τ) and amplitudes (α) of the different components of the fluorescence decays at different emission wavelengths of 1 in toluene, MeCN and MeCN with added TFA. Excitation occurred at 310 nm.

	Solvent	λ_{emi} (nm)	α_1 (%)	τ_1 (ns)	α_2 (%)	τ_2 (ns)
1	Tol	500			100	11.1
		650	100	1.9		
	MeCN	550			100	16.0
		700	97	0.29	3	16.0
1P$^+$	MeCN	550			100	4.76
		700			100	4.76

For molecule **2**, Peng et al. observed a small excitation wavelength dependency as well, but this was not reproduced in our results. Furthermore, the 2D plots (Figure 1E and 1F) show only one species in both solvents. The fact that **2** is less sensitive to protonation is probably due to the presence of the electron withdrawing benzonitrile moiety. This does not only reduce the basicity of N^1 but by resonance also that of N^3, the two most basic nitrogen atoms.

To further elaborate on the presence and absence of the dual emission in respectively **1** and **2**, an extensive computational study was performed. First, different conformers were optimized in the ground and excited states with (TD)-CAM-B3LYP, whereafter single point ADC(2) calculations were performed on top of these geometries to assess the accuracy of the TDDFT energies. As can be seen in Table S1, the TDDFT data deviate by less than 0.25 eV from the ADC(2) values, which is largely a systematic error, indicating that the TDDFT results are sufficiently accurate to predict correct trends. Therefore, all of the following results were obtained at the (TD)-CAM-B3LYP/6-31+g(d) level, using IEFPCM as solvent model. From the previous calculations (Table S1), it was also clear that the emission energies between conformers are very similar (~0.02 eV difference), excluding this already as a possible cause of the dual emission.

For the lower energy conformers, the calculated absorption, emission and zero-zero transition energies (ΔE^{00}, corresponding to the crossing point of normalized absorption and emission spectra) are compared with the main (lower energy) peak from the spectra, as is shown in Table 3. Computed values are on average overestimated by 0.15 eV compared to the experimental values, but all are within a 0.3 eV error margin, which is to be expected for TDDFT calculations. This shows that the long wavelength band of **1** corresponds to the transition to or from the S_1 state of the unprotonated form of **1**.

Table 3. Comparison of calculated (calc) and experimental (exp) values for absorption (abs), emission (emi) and zero-zero transition energies (ΔE^{00}). The latter is compared with the crossing point (cp) of the spectra. Experimental quantum yields (φ) and calculated oscillator strengths (f) are given as well. All energies are in eV, calculations were performed at the (TD)-CAM-B3LYP/6-31+g(d)/IEFPCM level.

	Solvent	$E_{abs,exp}$	$E_{abs,calc}$	cp	ΔE^{00}	$E_{emi,exp}$	$E_{emi,calc}$	φ	f
1	Tol	2.64	2.88	2.24	2.46	1.9	2.10	0.04	0.17
	MeCN	2.64	2.89	2.23	2.39	1.8	2.06	/	0.22
2	Tol	2.7	2.89	2.35	2.46	2.12	2.12	0.35	0.36
	MeCN	2.77	2.92	2.49	2.43	2.04	2.08	0.06	0.46

To further explain the dual emission, both the anti-Kasha scenario and different protonation mechanisms were explored computationally, in analogy with a similar BTD system investigated by Adele *et al*.[32] Intramolecular proton transfer (IPT), excited-state IPT (ESIPT) and intermolecular proton transfer (IePT) could all lead to protonated (indicated as **1**,**2**$P^+(N^X)$, with X = 1, 2 or 3 denoting the protonated nitrogen) or deprotonated (**1**,**2**DP^-) species. These processes could possibly be triggered by traces of water, acids or bases resulting from the syntheses, or by not using totally dry solvents. While deprotonation is only possible at the N^1 position, protonation can take place on all nitrogen atoms, see Scheme S1 for all investigated derivatives. The difference

between the two experimental emission maxima was compared with the calculated difference in emission energy, Δemi, for the different protonated and IPT species as well as for the anti-Kasha emission. Δemi is the difference between calculated values of the emission maxima of the different protonated or anti Kasha species and the calculated value of the $S_1 \rightarrow S_0$ emission maximum of the neutral molecules ($\Delta emi = emi_{protonated/IPT/AK} - emi_{neutral}$), hereby minimizing the influence of systematic errors. The same comparison was made for absorption (Δabs) and zero-zero transition energies ($\Delta\Delta E^{00}$), all of which are shown in Figure 3 and Table S2.

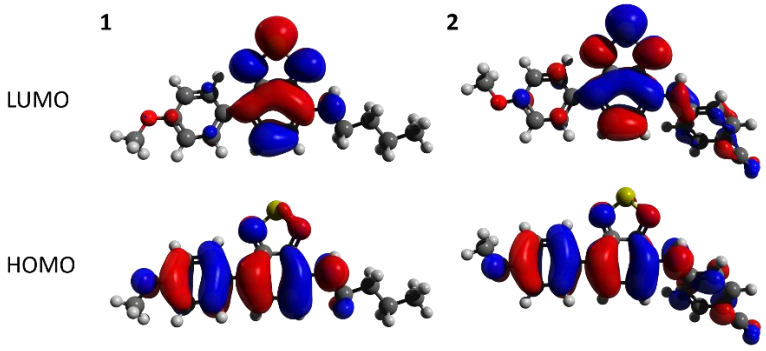

*Figure 2. Frontier molecular orbitals of **1** and **2** (CAM-B3LYP/6-31+G(d), MeCN).*

Before comparing the values, we elaborate a bit more on the type of orbitals involved in the excited states. In both molecules, the first excited state is a HOMO-LUMO (>95%) π-π*-transition, in which the HOMO is spread out over the whole molecule, whereas the LUMO is mainly located on the BTD-core (Figure 2). For the protonated species, the transitions are very similar, except for **2**$P^+(N^1)$, where the HOMO is not covering the PhCN-ring; and **2**$P^+(N^4)$, where the LUMO is delocalized over both the BTD-core and the PhCN-ring (Figure S6).

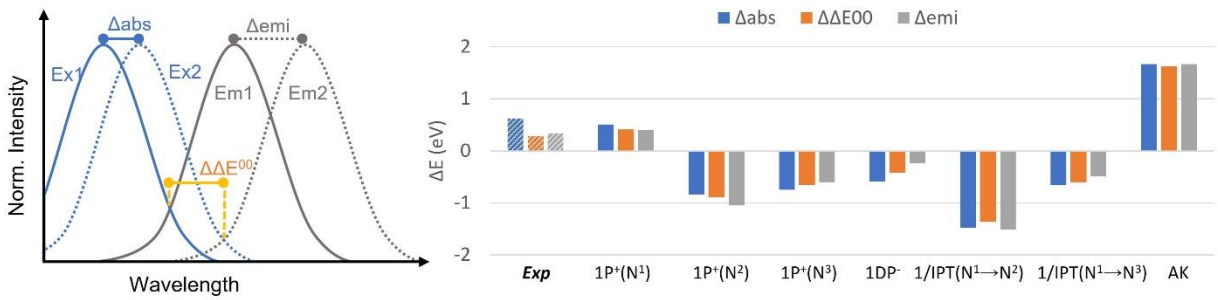

*Figure 3. Left: schematic image of compared energy differences. Right: comparison between different species and their predicted shift in fluorescence properties. 'Exp' is the experimental difference and 'AK' the difference in calculated properties between S_2 and S_1 of **1**.*

For **1**, both IPT($N^1 \rightarrow N^2$) and anti-Kasha (AK) emission (from S_2) the size of the differences deviates by >1 eV with respect to their experimental counterparts, making it unlikely that one of those is causing the dual emission. Next, the IPT($N^1 \rightarrow N^3$), the deprotonated and the BTD-protonated (N^2, N^3) species all predict a redshift, and although the energy differences are closer to the experiment, they are still underestimated by >0.5 eV. Lastly, the protonation on the amine group (N^1) predicts the same shift as the experiment within 0.12 eV, while our calculations also show that this is thermodynamically the most stable form of protonation for **1** (Table 4). In the excited state, **1**$P^+(N^2)$ and **1**$P^+(N^3)$ are more stable in energy, with **1**$P^+(N^2)$ being potentially protonated through an ESIPT process, leading us to compute the transition state (TS) between **1**$P^+(N^1)$ and **1**$P^+(N^2)$ (see computational details and Figure S7). Since the computed barrier is more than 17 kcal/mol, this process is probably too slow to compete with emission. As seen above, the experiments confirmed that a protonated form was indeed responsible for the blue-shifted peak, and hence concomitantly contributing together with the neutral form to the dual emission for **1**.

The experimental absence of dual emission for **2** is also in full agreement with our calculations, which predicts the protonation on the N^3 site to be the most stable. The small, computed emission energy from the latter tautomer (1.46 eV) along with its small oscillator strength, likely leads to a negligible radiative rate compared with the non-radiative rate. Furthermore, this form is thermodynamically less likely to be formed. This results in the absence of dual emission for this compound, having only fluorescence from the neutral form.

Table 4. Energy difference (kcal/mol) with respect to the lowest energy species in kcal/mol. Results are shown for calculations in acetonitrile (toluene). (TDCAM-B3LYP/6-31G(d))

	S_0	S_1		S_0	S_1
1	**0**	0	**2**	**0**	0
1/IPT($N^1 \rightarrow N^2$)	41 (43)	10 (/)[a]	**2**/IPT($N^1 \rightarrow N^2$)	35 (38)	3 (/)[a]
1/IPT($N^1 \rightarrow N^3$)	34 (36)	20 (25)	**2**/IPT($N^1 \rightarrow N^3$)	29 (31)	10 (14)
1$P^+(N^1)$	**0**	20 (24)	**2**$P^+(N^1)$	5 (7)	28 (31)
TS **1**$P^+(N^1) \rightarrow$ **1**$P^+(N^2)$		17 (/)[a]	**2**$P^+(N^2)$	4 (5)	2 (4)
1$P^+(N^2)$	12 (11)	2 (3)	**2**$P^+(N^3)$	**0**	0
1$P^+(N^3)$	4 (1)	0	**2**$P^+(N^4)$	12 (9)	28 (18)

[a] *Optimization not converged in toluene*

CONCLUSION

In summary, we showed that neither **1** nor **2** display anti-Kasha emission, and refute that emission from S_2 is the origin of the dual fluorescence in these compounds. Both steady state spectroscopic results and lifetime measurements indicate the presence of a protonated derivative in **1**, i.e., **1**$P^+(N^1)$, which is also confirmed by the exhaustive computational investigations. This shift in emission could however make **1** suitable as a pH sensor. Furthermore, we found that **1** most likely gets protonated on the amine group, while excited state intramolecular proton transfer is too slow

compared to direct emission. For **2**, the PhCN-group lowers the proton affinity of the amine group, explaining the absence of dual emission for this compound. This work serves as a reminder that it is important to take great care in assigning the mechanisms of anomalous photochemical phenomena. Hence, it is essential to have an agreement between both spectroscopic and computational methods.

Author Contributions

K.V.: Conceptualization, computational investigation, formal analysis, and writing (review and editing). F.d.J.: Conceptualization, spectroscopic investigation, formal analysis, and writing (review and editing). A.A.: Computational work. G.C.: Synthesis and characterization. K.C.: Spectroscopic experiments. Y.D.L.: Spectroscopic experiments. Q.M.: Computational work. T.P.: Synthesis and characterization. J.S.: Computational work. W.D.: Writing (review and editing) M.V.d.A.: Writing (review and editing) D.E.: Conceptualization, formal analysis, writing (review and editing), and funding acquisition.

Funding Sources

D.E. and K.V. acknowledge KU Leuven internal funds for financial support. F.d.J. thanks the Research Foundation-Flanders (FWO) for the FWO-SB fellowship 1SC4719N.

Keywords

Anti-Kasha, Benzothiadiazole, Computational Chemistry, Fluorescence, Spectroscopy

REFERENCES

(1) Peng, Z.; Wang, Z.; Huang, Z.; Liu, S.; Lu, P.; Wang, Y. Expression of Anti-Kasha's Emission from Amino Benzothiadiazole and Its Utilization for Fluorescent Chemosensors and Organic Light Emitting Materials. *J. Mater. Chem. C* **2018**, *6* (29), 7864–7873.

https://doi.org/10.1039/C8TC02416B.
(2) Kasha, M. Characterization of Electronic Transitions in Complex Molecules. *Discuss. Faraday Soc.* **1950**, *9* (c), 14. https://doi.org/10.1039/df9500900014.
(3) IUPAC. Isotopomer. In *IUPAC Compendium of Chemical Terminology*; IUPAC: Research Triagle Park, NC, 2014. https://doi.org/10.1351/goldbook.I03352.
(4) Braslavsky, S. E. Glossary of Terms Used in Photochemistry, 3rd Edition (IUPAC Recommendations 2006). *Pure Appl. Chem.* **2007**, *79* (3), 293–465. https://doi.org/10.1351/pac200779030293.
(5) Viswanath, G.; Kasha, M. Confirmation of the Anomalous Fluorescence of Azulene. *J. Chem. Phys.* **1956**, *24* (3), 574–577. https://doi.org/10.1063/1.1742548.
(6) Turro, N. J.; Ramamurthy, V.; Cherry, W.; Farneth, W. The Effect of Wavelength on Organic Photoreactions in Solution. Reactions from Upper Excited States. *Chem. Rev.* **1978**, *78* (2), 125–145. https://doi.org/10.1021/cr60312a003.
(7) Itoh, T. Fluorescence and Phosphorescence from Higher Excited States of Organic Molecules. *Chem. Rev.* **2012**, *112* (8), 4541–4568. https://doi.org/10.1021/cr200166m.
(8) Demchenko, A. P.; Tomin, V. I.; Chou, P.-T. Breaking the Kasha Rule for More Efficient Photochemistry. *Chem. Rev.* **2017**, *117* (21), 13353–13381. https://doi.org/10.1021/acs.chemrev.7b00110.
(9) Veys, K.; Escudero, D. Computational Protocol To Predict Anti-Kasha Emissions: The Case of Azulene Derivatives. *J. Phys. Chem. A* **2020**, *124* (36), 7228–7237. https://doi.org/10.1021/acs.jpca.0c05205.
(10) Koen, V.; Escudero, D. Anti-Kasha Fluorescence in Molecular Entities: Central Role of Electron−Vibrational Coupling. *Acc. Chem. Res.* **2022**, *XXXX* (XXX), XXX–XXX. https://doi.org/10.1021/acs.accounts.2c00453.
(11) del Valle, J. C.; Catalán, J. Kasha's Rule: A Reappraisal. *Phys. Chem. Chem. Phys.* **2019**, *21* (19), 10061–10069. https://doi.org/10.1039/C9CP00739C.
(12) Gierschner, J.; Behera, S. K.; Park, S. Y. Dual Emission: Classes, Mechanisms and Conditions. *Angew. Chemie Int. Ed.* **2020**, anie.202009789. https://doi.org/10.1002/anie.202009789.
(13) Welch, G. C.; Coffin, R.; Peet, J.; Bazan, G. C. Band Gap Control in Conjugated Oligomers via Lewis Acids. *J. Am. Chem. Soc.* **2009**, *131* (31), 10802–10803. https://doi.org/10.1021/ja902789w.
(14) Neto, B. A. D.; Lapis, A. A. M.; da Silva Júnior, E. N.; Dupont, J. 2,1,3-Benzothiadiazole and Derivatives: Synthesis, Properties, Reactions, and Applications in Light Technology of Small Molecules. *European J. Org. Chem.* **2013**, *2013* (2), 228–255. https://doi.org/10.1002/ejoc.201201161.
(15) Baekelant, W.; Aghakhani, S.; Coutino-Gonzalez, E.; Grandjean, D.; Kennes, K.; Jonckheere, D.; Fron, E.; D'Acapito, F.; Longo, A.; Lievens, P.; Roeffaers, M. B. J.; Hofkens, J. Confinement of Highly Luminescent Lead Clusters in Zeolite A. *J. Phys. Chem. C* **2018**, *122* (25), 13953–13961. https://doi.org/10.1021/acs.jpcc.8b01107.
(16) Salahub, D. R.; Zerner, M. C. ChemInform Abstract: The Challenge of d and f Electrons. Theory and Computation. *ChemInform* **1990**, *21* (33). https://doi.org/10.1002/chin.199033368.
(17) Hohenberg, P.; Kohn, W. Inhomogeneous Electron Gas. *Phys. Rev.* **1964**.

https://doi.org/10.1103/PhysRev.136.B864.
(18) Kohn, W.; Sham, L. J. Self-Consistent Equations Including Exchange and Correlation Effects. *Phys. Rev.* **1965**. https://doi.org/10.1103/PhysRev.140.A1133.
(19) CASIDA, M. E. Time-Dependent Density Functional Response Theory for Molecules; 1995; pp 155–192. https://doi.org/10.1142/9789812830586_0005.
(20) Runge, E.; Gross, E. K. U. Density-Functional Theory for Time-Dependent Systems. *Phys. Rev. Lett.* **1984**, *52* (12), 997–1000. https://doi.org/10.1103/PhysRevLett.52.997.
(21) Hehre, W. J.; Ditchfield, R.; Pople, J. A. Self—Consistent Molecular Orbital Methods. XII. Further Extensions of Gaussian—Type Basis Sets for Use in Molecular Orbital Studies of Organic Molecules. *J. Chem. Phys.* **1972**, *56* (5), 2257–2261. https://doi.org/10.1063/1.1677527.
(22) Yanai, T.; Tew, D. P.; Handy, N. C. A New Hybrid Exchange–Correlation Functional Using the Coulomb-Attenuating Method (CAM-B3LYP). *Chem. Phys. Lett.* **2004**, *393* (1–3), 51–57. https://doi.org/10.1016/j.cplett.2004.06.011.
(23) Li, X.; Frisch, M. J. Energy-Represented Direct Inversion in the Iterative Subspace within a Hybrid Geometry Optimization Method. *J. Chem. Theory Comput.* **2006**, *2* (3), 835–839. https://doi.org/10.1021/ct050275a.
(24) Tomasi, J.; Mennucci, B.; Cammi, R. Quantum Mechanical Continuum Solvation Models. *Chem. Rev.* **2005**, *105* (8), 2999–3094. https://doi.org/10.1021/cr9904009.
(25) Dreuw, A.; Wormit, M. The Algebraic Diagrammatic Construction Scheme for the Polarization Propagator for the Calculation of Excited States. *Wiley Interdiscip. Rev. Comput. Mol. Sci.* **2015**, *5* (1), 82–95. https://doi.org/10.1002/wcms.1206.
(26) Weigend, F.; Häser, M.; Patzelt, H.; Ahlrichs, R. RI-MP2: Optimized Auxiliary Basis Sets and Demonstration of Efficiency. *Chem. Phys. Lett.* **1998**, *294* (1–3), 143–152. https://doi.org/10.1016/S0009-2614(98)00862-8.
(27) TURBOMOLE V7.1 2016, a Development of University of Karlsruhe and Forschungszentrum Karlsruhe GmbH, 1989-2007, TURBOMOLE GmbH, since 2007; Available from Http://Www.Turbomole.Com.
(28) Frisch G. W.; Schlegel, H. B.; Scuseria, G. E.; Robb, M. A.; Cheeseman, J. R.; Scalmani, G.; Barone, V.; Petersson, G. A.; Nakatsuji, H.; Li, X.; Caricato, M.; Marenich, A. V.; Bloino, J.; Janesko, B. G.; Gomperts, R.; Mennucci, B.; Hratch, D. J., M. J. . T. Gaussian 16, Rev. A.03. *Gaussian, Inc., Wallingford, CT* **2016**. https://doi.org/111.
(29) Qin, W.; Rohand, T.; Baruah, M.; Stefan, A.; der Auweraer, M. Van; Dehaen, W.; Boens, N. Solvent-Dependent Photophysical Properties of Borondipyrromethene Dyes in Solution. *Chem. Phys. Lett.* **2006**, *420* (4–6), 562–568. https://doi.org/10.1016/j.cplett.2005.12.098.
(30) Pevenage, D.; Corens, D.; Dehaen, W.; der Auweraer, M.; De Schryver, F. Influence of the N-Substituent on the Photophysical Properties of Oxacarbocyanines in Solution. *Bull. des Sociétés Chim. Belges* **1997**, *106* (9), 565–572.
(31) Van der Auweraer, M.; Van den Zegel, M.; Boens, N.; De Schryver, F. C.; Willig, F. Photophysics of 2-Phenyl-3-Indolocarbocyanine Dyes. *J. Phys. Chem.* **1986**, *90* (6), 1169–1175. https://doi.org/10.1021/j100278a041.
(32) Laurent, A. D.; Houari, Y.; Carvalho, P. H. P. R.; Neto, B. A. D.; Jacquemin, D. ESIPT or Not ESIPT? Revisiting Recent Results on 2,1,3-Benzothiadiazole under the TD-DFT Light. *RSC Adv.* **2014**, *4* (27), 14189–14192. https://doi.org/10.1039/C4RA00991F.

TOC:

Computational and spectroscopic investigation of the anomalous fluorescence of two benzothiadiazole derivatives. The originally assigned anti-Kasha mechanism could not be confirmed, but instead separate emission from a protonated form was suggested.